A novel methodological approach for achieving £/MWh cost reduction of CO_2 capture and storage (CCS) processes

Renato P. Cabral[a,b], Niall Mac Dowell[b,c,*]

[a]*SSCP DTP, Grantham Institute for Climate Change and the Environment, Imperial College London, South Kensington, London, SW7 2AZ, UK*
[b]*Centre for Environmental Policy, Imperial College London, South Kensington, London, SW7 1NA, UK*
[c]*Centre for Process Systems Engineering, Imperial College London, South Kensington, London, UK SW7 2AZ*

Abstract

Carbon capture and storage is widely recognised as essential for the cost effective decarbonisation of the power and industrial sectors. However its capital and operating costs remains a barrier to deployment, with significant reduction in the cost per unit of decarbonised product considered vital. In the context of power generation, this is best expressed in terms of cost per MWh of electricity generated. To achieve a meaningful reduction in the cost of low carbon electricity, capital costs must also be reduced. Thus, this work presents a novel approach for identifying system improvements via a combination of process integration and intensification based on minimisation of thermodynamic losses. Application of this methodology to an oxy-combustion CCS process led to a 3% increase of net efficiency and a 13% reduction of £/MWh of electricity.

Keywords: Oxy-combustion, Cryogenic distillation, Carbon capture and storage, Exergy analysis, Techno-economic analysis, Heat integration

*Corresponding author
  Email address:* `niall@imperial.ac.uk` (Niall Mac Dowell)

1. Introduction

Anthropogenic carbon dioxide (CO_2) emissions from burning fossil fuels are currently recognised as the leading contributor to climate change, with 36.2 Gt being emitted in 2015 [1, 2]. However, despite substantial investment in renewable energy, fossil fuels continue to play an integral role in the world's energy landscape [3]. Indeed, coal still plays a major role as a primary energy source [4] and although its global use is declining, some countries are highly reliant on this fuel, so it is expected that coal will keep being relevant in the future.

Carbon capture and storage (CCS) technologies have the potential to reduce these anthropogenic CO_2 emissions as part of a transition to a low carbon energy system [5–7]. These technologies are typically divided in three categories: pre-combustion, post-combustion, and oxy-combustion [6, 8], and all are based on the idea of the capture and subsequent storage of CO_2 from the combustion of fossil fuels in either the power or industrial sectors. In all cases, high purity CO_2 has to be compressed to approximately 110 bar prior to transportation via pipeline to a storage site [9–11][1].

Oxy-combustion is a promising technology where fuel is burnt in a high-oxygen (O_2) environment, using O_2 obtained from an air separation unit (ASU), instead of with air, improving combustion efficiency [12]. Safe operation conditions are maintained by recycling a fraction of the flue gas back to the furnace, thus keeping the temperatures inside the boiler close to air-firing mode [9, 13–15]. Burning coal under these conditions generates an flue gas rich in CO_2 (60-70 mol%) with appreciable quantities of H_2O (20-25 mol%), O_2 (3-4 mol%) and N_2 (0-10 mol%), which varies according to coal rank and process design [13]. This flue gas is then upgraded to transport specifications via a gas processing unit (GPU) [7, 14, 16].

---

[1]Actual compression pressure is a function of the design of the CO_2 transport infrastructure and the chosen CO_2 storage option.

Oxy-combustion can also be applied to natural gas combined cycle (NGCC), however the gas turbines need to be redesigned because the increased CO_2 concentrations in the flue gas alter its physical properties [9, 12]. Unlike for pulverized coal oxy-combustion, O_2 must be compressed to the high operating pressures of the NGCC before delivered to the furnace [9].

Currently, the dominant technology for producing the quantities of oxygen required for oxy-combustion of pulverized coal (above 600 kg/MWh)[2] is cryogenic distillation [17, 18]. This technology was originally commercialised by Carl von Linde in 1902 [19] and is based on separation of the constituents of air using distillation at cryogenic temperatures [20–25]. Despite its technical maturity, cryogenic distillation processes are still energy intensive consuming 200 kWh/t_{O_2} [26] which led to proposals for reducing this penalty, such as using self-heat recuperation [27]. This high energy requirement also promoted the development of alternative technologies for air separation, such as adsorption [28–30], ion transport membranes (ITM) [31–35], and chemical looping [36–38]. However, none of these technologies are suitable for the production of high purity oxygen at utility scale either because of high costs, as for adsorption processes, or the technology is still under development, as for ITM [17, 39].

The requirement to add both an ASU and GPU increases the capital cost of the plant and imposes an 8 - 12% efficiency penalty to the process [7, 40]. One way of minimising the effects of this efficiency penalty is through heat integration, which can be optimised by minimising inefficiencies within the process via an exergy destruction analysis. This analysis is based on the second law of thermodynamics, aimed at identifying inefficiencies within a system due to irreversibility [41]. Exergy refers to the amount of work that can be generated by a system on a reversible process, leaving it in equilibrium with the environment [42].

Several studies have focused on reducing this parasitic power consumption by performing thermodynamic and techno-economic analyses on double and

---

[2]This equates to a rate of 7200 t_{O_2}/day for a 500 MW power plant.

3

triple column ASUs, and different GPU units [43–45]. Skorek-Osikowska *et al.* determined that low grade heat of compression could be used to pre-heat the feedwater reducing the number of feedwater heaters required [45]. Aneke *et al.* simulated an oxy-combustion process with liquid air storage and determined there was an advantage to using this strategy as well as recovering waste heat of compression [46]. Stanger *et al.* and Li *et al.* both determined that SO_x can have higher concentrations in oxy-combustion flue gas than in air-combustion due to recycling and a lack of dilution by N_2 [47, 48]. This increase in SO_x has the effect of increasing acid dew point from $116\,°C$ in air-firing to $141.6\,°C$ in oxy-combustion [47], as well as changes in ash composition [48, 49]. Oxy-combustion CCS has been demonstrated a number of times, including the Callide oxyfuel project [50–52], Lacq pilot plant [53], Compostilla OXYCFB300 circulating fluidised bed [54], and Vattenfall's pilot plant [55, 56]. These projects proved the feasibility of oxy-combustion and provided further insights on operational performance of the technology.

Whilst improvements in process performance are important, it is vital that they do not result in increased capital cost, leading to an increased cost per MWh of low carbon electricity generated. This creates the need to develop a methodological approach that allows the evaluation of the efficacy of a process modification in this context.

In this work, we present a novel methodological approach for the identification and rational analysis of potential process performance improvements via system integration and process intensification. This approach is grounded in the application of the 1st and 2nd laws of thermodynamics coupled with a capital expenditure (CAPEX) analysis. The methodology proposed in this study is well-suited for application to other CCS technologies, or more generally to other complex industrial processes, such as liquefied natural gas processes.

2. Methods

2.1. General model

All models in this study were implemented in Aspen HYSYS v8.4 and all thermophysical properties were calculated using the Peng-Robinson equation of state fluid package. The process flow diagram (PFD) of the oxy-combustion is presented in schematic form in Figure 1.
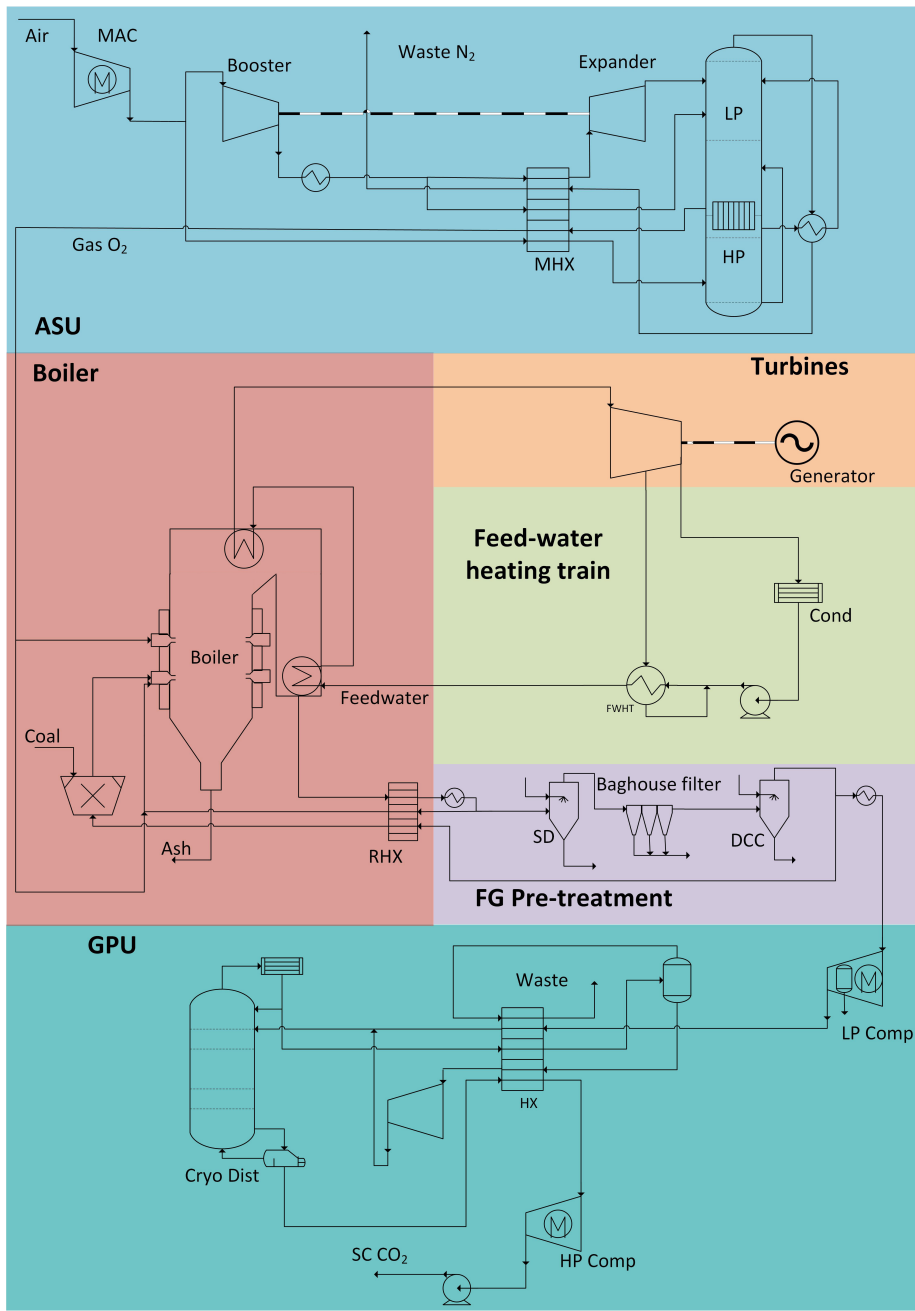
Figure 1: Process Flow Diagram (PFD) of the oxy-combustion process without heat integration. The process consists of a double column cryogenic ASU for O_2 production, a pulverised coal boiler with flue gas treatment plant, and cryogenic GPU.

A medium sulphur bituminous coal with a grindability of 0.664 g/rev [57] was used in this work with the composition detailed in Table 1. The power required, W (kWh/t), to grind coal with mean particle size of 2.7 mm (F_{80}) to a target size of 90 μm (P_1) and mean particle size of 77 μm (P_{80}) is given by Equations 1 and 2 [57],

$$W = 10 \ W_i \left(1/\sqrt{P_{80}} - 1/\sqrt{F_{80}} \right) \tag{1}$$

$$W_i = \frac{44.5}{P_1^{0.23} \ G^{0.82} \ \left(10/\sqrt{P_{80}} - 10/\sqrt{F_{80}} \right)} \tag{2}$$

Table 1: Composition of bituminous coal used in this work, obtained from IECM program [58].

Fuel Component	Mass Fraction (w_i)
C	0.74
H	0.05
S	0.02
O	0.05
N	0.01
H_2O	0.05
Cl_2	6×10^{-4}
Ash	0.07
Fuel HHV (MJ/kg)	33.48

2.2. Air Separation Unit (ASU)

The double column ASU was modelled following the work of Sapali and Raibhole [24, 25] as illustrated in Figure 2. Air is compressed to 4.2 bar by the main air compressor (MAC), simulated as a five-staged isothermal compressor with inter-coolers to keep air temperature at 25 °C. Compressed air is cooled in a heat exchanger (HX1) to 45 °C and 25% of this stream is compressed to

7

50 bar by a booster compressor partly powered by an expansion turbine. This stream is cooled to 45 °C in HX2 and 9% is sent to the main heat exchanger (MHX) of the plate-fin type to be cooled to 10 °C and sent to the Expander. This step generates the required cooling to operate the plant, sending air at 1.25 bar and −171.4 °C to the low pressure (LP) column with 56 theoretical stages. The compressed air stream not sent to the booster is sent to the MHX, cooled to −179 °C and expanded by a Joule-Thomson valve, not shown to keep simplicity of the PFD, to 1.25 bar and −192 °C before entering the LP column. The stream bypassing the Booster is cooled to −178 °C and partially condensed in the MHX before being sent to the high pressure (HP) column with 40 theoretical stages for pre-separation of O_2 and N_2 [20–25]. The operating parameters of the ASU are presented in Table 2.
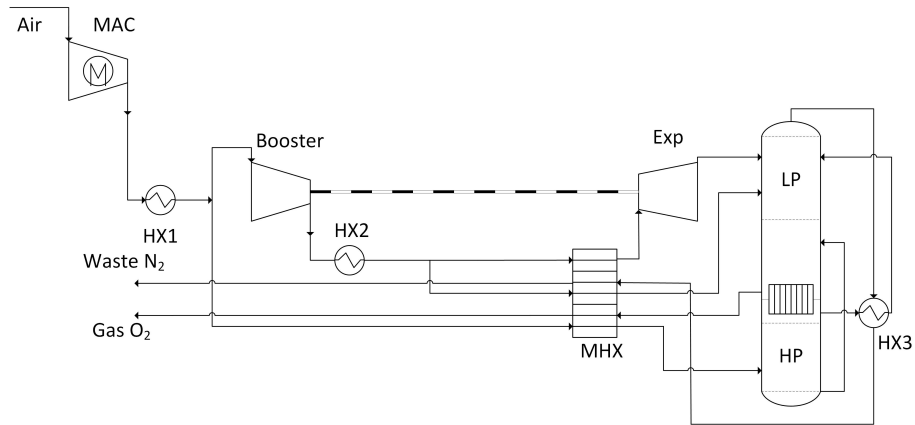

Figure 2: Process Flow Diagram (PFD) of the double column cryogenic ASU for O_2 production. MAC - Main air compressor; Booster - Booster compressor; Exp - Expander; HX1 and HX2 - Coolers; MHX - Main heat exchanger; HX3 - Subcooler; HP - High pressure column; LP - Low pressure column.

Table 2: Operating parameters of the ASU, as well as feed compositions.

Parameter	Unit	Value
Air temperature at the inlet to the ASU	°C	10
Air pressure at the inlet to the ASU	bar	1.01
Molar composition of air		
N_2	mol%	78
O_2	mol%	20
Ar	mol%	1
Air temperature at the outlet of the inter-coolers	°C	28
Pressure in the HP column	bar	4.1
O_2 purity leaving the bottom of the HP column	%	39
Pressure in the LP column	bar	1.1
Isentropic efficiency of the MAC	%	85

An air stream enriched with 39 wt% of O_2 exits through the bottom of the HP column at 4.1 bar and is then expanded to 1.25 bar before entering the LP column. On the top of the HP column, high purity N_2 is condensed against boiling O_2 from the sump of the LP column in a condenser/reboiler that allows a temperature difference as low as 0.4 °C [59]. Liquid N_2 produced in the HP column is cooled in a subcooler (HX3) against waste N_2 from the top of the LP column. This stream is expanded to 1.25 bar before being used in the LP column to provide its required reflux. The double column was modelled as two separate distillation columns with the condenser of the HP column connected to the reboiler of the LP column to simulate the condenser/reboiler. Waste N_2 is obtained from the top of the LP column, has its temperature increased in HX3, and is sent to the MHX. A stream of high purity O_2 (97 wt%) is obtained from the bottom of the LP column and is sent to the MHX. Here, liquid O_2 reduces the temperature of incoming air in conjunction with waste N_2, leaving as a gas at 38 °C to be used on the combustion chamber [20–23, 25].

2.3. Power plant

The ultra-supercritical power plant was first simulated operating in air-fired mode based on the Callide oxyfuel project [50] and Spliethoff [60], as seen in Figure 3. It is a pulverised coal-fired plant composed of a two-pass once-through boiler [61], a turbine island, a feedwater heating train, and a flue gas pre-treatment unit. Air is pre-heated to 268 °C by recovering heat from the flue gas exiting the boiler at 381 °C and then this hot air stream is sent to the mill, pulverising coal to the furnace. The combustion of coal takes place here and is simulated as a conversion reactor where coal is oxidized and CO_2, H_2O, SO_2, and SO_3 are produced. The mass flow of ash, including both bottom and fly ash, was specified to be 30% of the fuel mass, representing a high ash coal scenario, with Spero reporting 24% ash in Callide coal [50]. Fly ash goes into the boiler section along with flue gas while the remaining furnace ash falls down to an ash hopper [50]. Feedwater is heated against hot flue gas in the boiler, comprised of the Evaporator (Evap), Radiant Superheater (RS), Superheater 2 (SH2), Reheater 2 (RH2), Superheater 1 (SH1), Reheater 1 (RH1), and Economiser (Econ). These components were modelled as heat exchangers following the paths shown in the boiler section of Figure 3. Flue gas is then cooled against incoming air to 130 °C in a regenerative heat exchanger (RHX) [44, 61]. This temperature is chosen to be above acid dew point [9, 50] and allows a safe operation for baghouse filters [50]. The operating parameters of the power plant are presented in Table 3.

Table 3: Boiler and flue gas pre-treatment operating conditions.

| Parameter	Unit	Value
Feedwater temperature	°C	299
Steam temperature at superheater exit	°C	600
Reheated steam temperature at reheater exit	°C	620
Steam pressure at superheater exit	bar	300
Steam pressure at reheater exit	bar	70
Excess air ratio		1.04
Amount of ash in coal	wt%	30
Amount of fly ash in total ash	wt%	90
Isentropic efficiency of fans	%	85
Isentropic efficiency of compressors	%	75
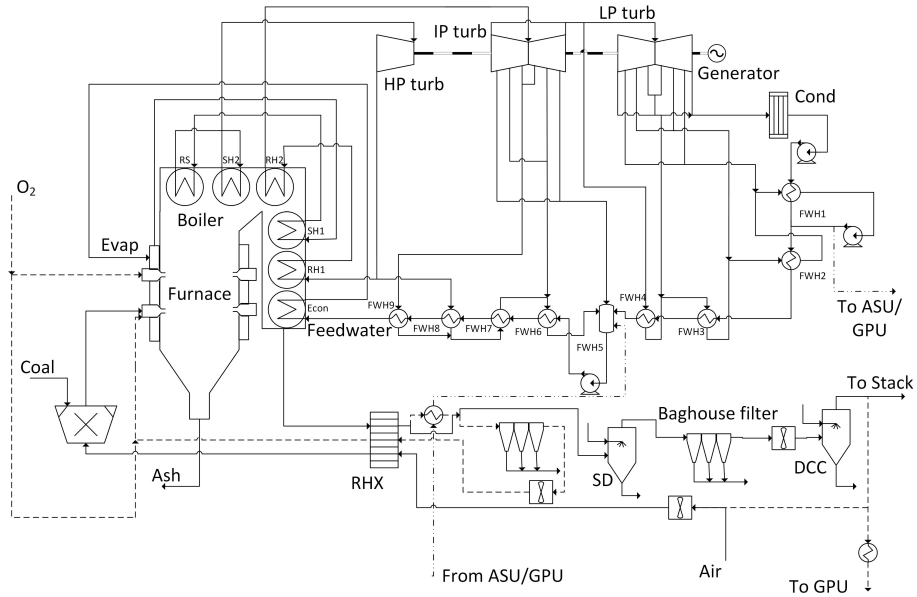
Figure 3: Process Flow Diagram (PFD) of the power plant complete with coal mill, boiler, turbine, feedwater heating train, ash collection and flue gas desulphurisation. The boiler is divided into two sections: the furnace, where combustion takes place, and the boiler, where heat increases the temperature of feedwater and generate supercritical steam. Solid lines represent the flow paths in air- and oxy-modes, except for air inlet which is present in air-mode only. Dashed lines represent the extra flow paths in oxy-mode for O_2 feed and RFG. Dashed and dotted lines represent the heat integration pathways between the feedwater heating train and the compressors from the ASU and GPU. Feedwater heaters 1 to 4 can be bypassed with heat integration. HP turb - High pressure turbine; IP turb - Intermediate pressure turbine; LP turb - Low pressure turbine; Cond - Condenser; Econ - Economiser; Evap - Evaporator; SH1 and SH2 - Superheater 1 and 2; RS - Radiant superheater; RH1 and RH2 - Reheater 1 and 2, FWH1 to FWH9 - Feedwater heater 1 to 9; RHX - Regenerative heat exchanger; SD - Spray dryer for desulphurization.

Feedwater enters the boiler through the economiser and leaves through SH2 where it is sent to the high pressure turbine (HP turb) at 600 °C and 300 bar. Part of the steam is used to pre-heat feedwater and the remainder is reheated in the boiler. The pressure drop of the flue gas inside the boiler was assumed to be 2.1 mbar, while feedwater had a pressure drop of 24.1 bar for the economiser,

evaporator, and superheaters sections, and 5 bar for the reheater section[9]. Steam exits the boiler from RH2 at 620 °C and is expanded inside an intermediate pressure turbine (IP turb) followed by a low pressure turbine (LP turb) to 0.04 bar. The amount of steam bled from each turbine, as well as their conditions, is presented in Table 4. Steam leaving the LP Turb is condensed and pumped to the feedwater heating train, where it is heated to 299 °C against the turbine bleeds, and sent back to the boiler.

Table 4: Fractions and conditions of steam bled from the HP, IP and LP turbines, based on turbine feed to reach feedwater temperature of 299 °C.

Turbine	bleed no	w_n (%)	T (°C)	P (bar)
HP	1	9.30	365	75
IP	1	7.45	558	48
	2	4.81	460	25
	3	4.54	381	14
	4	4.82	297	7
LP	1	9.60	200	2.8
	2	5.60	102	0.9
	3	4.64	65	0.25

2.4. Gas Processing Unit (GPU)

A GPU process based on a combination of compression and distillation was simulated following the work of Posch *et al.* [62]. Flue gas at 26 °C and 1.01 bar enters the first compressor (LP Comp1), where it is compressed to 10.1 bar and then cooled to 20 °C in cooler HX1. This flue gas is sent to a flash separator (flash-1) where the condensate, mostly water, is removed from the gas [63–65]. The gas phase is further compressed to 20 bar in the second compressor (LP Comp2) and cooled to 25 °C in HX2 and sent to another flash separator (flash-2) where more water is removed from the gas phase. This gas phase is compressed to 28 bar in compressor LP Comp3, cooled again to 25 °C in HX3 and sent to

13

another flash separator (flash-3) for more water removal.

Compressed flue gas is sent to a dehydrator for water removal [62] and subsequently cooled against cold products from the distillation column to $-31\,^{\circ}\mathrm{C}$ in a multiple stream heat exchanger (MHX) of plate-fin type. The cooled stream is mixed with the recycled stream and fed to the distillation column where high-purity CO_2 (99.96 wt%) is obtained.

From the top of the distillation column (Cryo Dist), an impure CO_2 stream is sent to the MHX and then to a flash separator (flash-4). A CO_2 rich liquid is recycled back to the distillation column and the gas phase is sent to the stack after cooling incoming flue gas on the MHX. Pure stream of CO_2 is warmed in the MHX and compressed to 68 bar and $1\,^{\circ}\mathrm{C}$ by a multiple staged compressor (HP Comp1 and 2) with inter- and after-cooling (HX5 and 6). This stream is further compressed to 120 bar and $5\,^{\circ}\mathrm{C}$ by a pump (P-1) and sent to the pipeline, as represented in Figure 4. The operating parameters of the GPU are presented in Table 5.
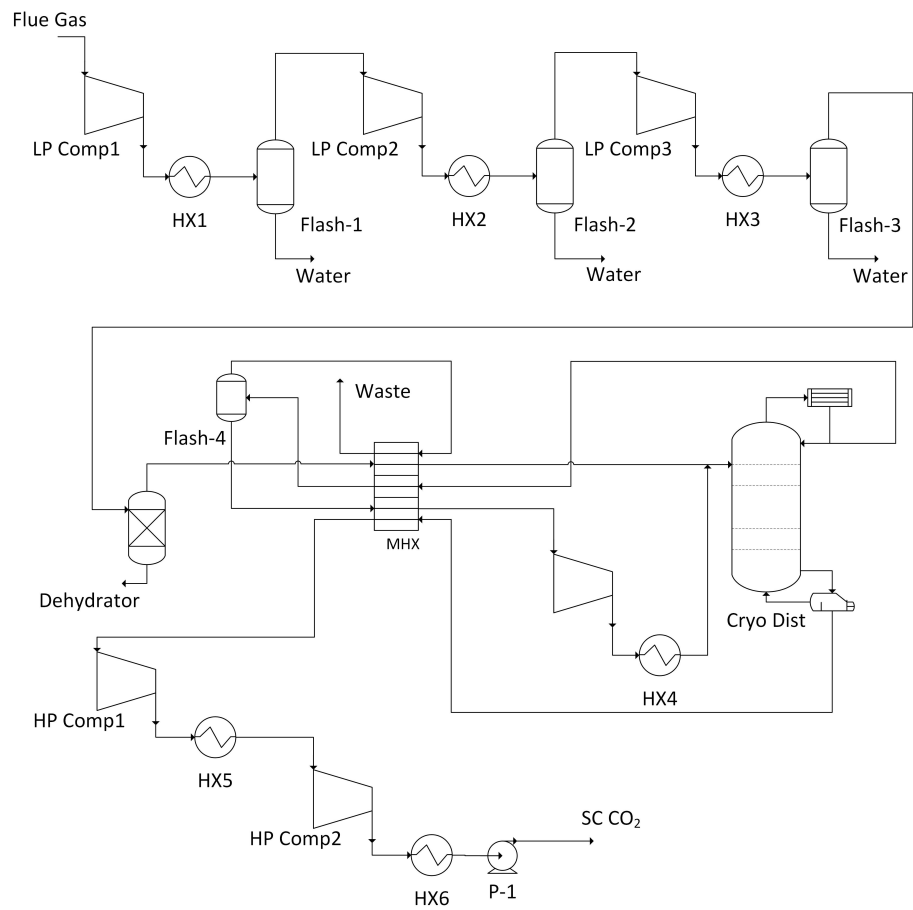
Figure 4: Process Flow Diagram (PFD) of the GPU. LP Comp1 to LP Comp3 - Low pressure compressors 1 to 3; HX1 to HX6 - Coolers; MHX - Multiple heat exchanger; Flash-1 to Flash-4 - Flash separator 1 to 4; Cryo Dist - Distillation column; P-1 - Pump.

Table 5: GPU operating conditions.

Parameter	Unit	Value
Flue gas pressure at GPU inlet	bar	1.01
Flue gas temperature at GPU inlet	°C	26
Flue gas molar composition at GPU inlet		
CO_2	%	87.36
O_2	%	5.07
N_2	%	1.64
SO_2	%	0.02
H_2O	%	3.1
Ar	%	2.81

2.5. Oxy-combustion

The simulation of an oxy-combustion process was modelled following the work of Spero *et al.* [50] and Stanger *et al.* [66]. The power plant model developed previously was adapted with a primary and secondary recycle flue gas (RFG) to the furnace. The O_2 supplied by the ASU is mixed with the secondary RFG to keep O_2 concentration below 40% to avoid the use of construction materials specific for pure O_2 [9]. Flue gas leaves the boiler and pre-heats RFG in a regenerative heat exchanger (RHX), and 52% of total FG is mixed with the O_2 stream in what is commonly called the secondary recycle, and sent back to the furnace. An additional baghouse filter on the secondary RFG is required to avoid a buildup of fly ash inside the boiler. The rest of the flue gas is sent to a spray dryer (SD) for SO_x removal, passed through another baghouse filter to remove fly ash, and cooled in a direct contact cooler (DCC) [7, 50, 65, 67]. 37% of this flue gas is recycled as the primary RFG and used to pulverise ground coal to the furnace [50, 66]. The non-recycled flue gas is subsequently purified and compressed to transport specifications [68] on the gas processing unit (GPU) [16, 50]. The resulting PFD of the boiler operating in oxy-mode is

presented in Figure 3.

2.6. Heat integration

Heat integration was performed by pre-heating feedwater leaving the condenser using low grade heat of compression of the ASU and GPU as represented in Figure 3[44, 45]. The minimum allowable temperature at the regenerative heat exchanger outlet was defined as 150 °C to be above acid dewpoint [47]. Medium temperature feedwater incoming from the ASU can be used to further cool down the flue gas before particulate removal. Using this heat integration strategy allows elimination of feedwater heaters 1 to 4, requiring less turbine bleeds and hence more steam to expand in the turbines to generate more electricity. The bleed fractions for the process with heat integration are presented in Table 6.

Table 6: Fractions and conditions of steam bled from the HP, and IP turbines, based on turbine feed to reach feedwater temperature of 299 °C.

Turbine	bleed no	w_n (%)	T (°C)	P (bar)
HP	1	9.30	365	75
IP	1	7.45	558	48
	2	4.81	460	25
	3	9.96	381	14

2.7. Thermodynamics analysis

A thermodynamic analysis was performed in order to determine the potential for an improvement to the gross and net efficiency of the process using Equations 3 and 4,

$$\eta_{gross} = \frac{P_{turbines}}{\dot{m}_{fuel} LHV} \tag{3}$$

$$\eta_{net} = \frac{P_{turbines} - P_{consumed}}{\dot{m}_{fuel} LHV} \tag{4}$$

17

The power generated by the turbines ($P_{turbines}$) is the sum of the power generated by the HP, IP and LP turbines. The power consumed ($P_{consumed}$) is the sum of the power demand of the ASU, the GPU, and from the fans and pumps circulating flue gas and feedwater respectively. The heat input of the fuel is taken by multiplying the lower heating value (LHV) and coal mass flow ($\dot{m}_{fuel}$). In this study, gross and net efficiencies were determined on a LHV basis.

The net efficiency was compared against the maximum thermodynamic efficiency that could be achieved using an ideal Rankine cycle and the minimum thermodynamic separation work for both ASU and GPU. The ideal Rankine cycle is determined using the Carnot efficiency with Equation 5,

$$\eta_{Rankine}^{Max} = 1 - \frac{T_{condenser}}{T_{Superheater}} \tag{5}$$

The Carnot efficiency reflects the amount of thermal energy that could be transformed to electricity assuming a hot source (Superheater) and a cold sink (condenser) with no losses in the system. It states that the limit of efficiency is driven by the source and sink absolute temperatures, $T_{Superheater}$ and $T_{condenser}$ respectively. With Equations 3 and 5 it is possible to calculate the maximum amount of power generated by the turbines ($P_{Rankine}^{Max}$)from a Rankine cycle.

The minimum thermodynamic work required to separate O_2 from air is given by Equation 6 and to separate CO_2 from flue gas by Equation 7,

$$
\begin{aligned}
W_{min}^{O_2}(kJ/mol) = {}& RT\left(n_{Oxy}^{O_2}\ln(y_{Oxy}^{O_2}) - n_{Oxy}^{Oxy-O_2}\ln(y_{Oxy}^{Oxy-O_2})\right) \\
& +RT\left(n_{Nit}^{O_2}\ln(y_{Nit}^{O_2}) - n_{Nit}^{Nit-O_2}\ln(y_{Nit}^{Nit-O_2})\right) \\
& -RT\left(n_{Air}^{O_2}\ln(y_{Air}^{O_2}) - n_{Air}^{Air-O_2}\ln(y_{Air}^{Air-O_2})\right)
\end{aligned}
\tag{6}
$$

$$
\begin{aligned}
W_{min}^{CO_2}(kJ/mol) = {}& RT\left(n_{Final}^{CO_2}\ln(y_{Final}^{CO_2}) - n_{Final}^{Final-CO_2}\ln(y_{Final}^{Final-CO_2})\right) \\
& +RT\left(n_{Waste}^{CO_2}\ln(y_{Waste}^{CO_2}) - n_{Waste}^{Waste-CO_2}\ln(y_{Waste}^{Waste-CO_2})\right) \\
& -RT\left(n_{FlueGas}^{CO_2}\ln(y_{FlueGas}^{CO_2}) - n_{FlueGas}^{FlueGas-CO_2}\ln(y_{FlueGas}^{FlueGas-CO_2})\right)
\end{aligned}
\tag{7}
$$

In Equations 6 and 7, Oxy refers the stream rich in O_2; Nit refers to the stream rich in N_2; Air refers to air inlet stream; Final refers to the stream rich in CO_2; Waste refers to the stream sent to the stack; and Flue Gas is the incoming flue gas. The minimum separation work (W_{min}) relates the molar flow of the component to be separated from the inlet and outlet streams at a certain operating temperature, in K. The gas constant R is 8.314 kJ K^{-1}kmol^{-1}.

The Second Law efficiency determined by Equation 8 shows the potential for improving the process,

$$\eta_{2nd} = \frac{W_{min}}{W_{real}} \tag{8}$$

Using the maximum power produced by a Rankine cycle and the minimum separation work determined by Equations 6 and 7, the maximum thermodynamic efficiency of oxy-combustion can be determined with Equation 9,

$$\eta_{net}^{Max} = \frac{P_{turbines}^{Max} - n_{Oxy}^{O_2} W_{min}^{O_2} - n_{Final}^{CO_2} W_{min}^{CO_2}}{\dot{m}_{fuel} LHV} \tag{9}$$

2.8. Exergy analysis

The previous analysis quantifies by how much it is possible to improve the process efficiency, but it does not give a clear indication of the units responsible for most irreversible losses. This insight can be obtained via an exergy destruction (ED) analysis for each unit operation using Equation 10,

$$ED = \sum_{In}(n(h-T_0 s) + Q(1-\frac{T_0}{T_s}) + W_s) - \sum_{Out}(n(h-T_0 s) + Q(1-\frac{T_0}{T_s}) + W_s) \tag{10}$$

The term $n(h-T_0 s)$ refers to the exergy of the stream, the term $Q(1-T_0/T_s)$ refers to the thermal energy that could be transformed into exergy using a Carnot cycle, n is the molar flow of the stream, h is the specific molar enthalpy, s is the specific molar entropy, T_0 is the reference temperature, T_s is the system temperature, and W_s is the work done to or by the system. Performing this analysis to each unit operation of oxy-combustion allows for the identification of the most suitable candidates for process improvement.

3. Results and Discussion

3.1. Simulation and model validation

Combustion is assumed to take place at an adiabatic flame temperature (T_{ad}) of 2167 °C, similar to the value reported by Lackner for anthracite of 2180 °C [69]. The simulated oxy-combustion process has a gross efficiency of 47.2% and a net efficiency of 34.6%, resulting in a 12% efficiency loss when compared with the unabated power plant. A good agreement between the simulated process and the results from IECM [58] and Callide oxyfuel project [51] was obtained, as presented in Table 7. The disagreement observed for O_2 demand and fuel burned is due to the assumption that complete combustion took place with no carbon monoxide (CO) formation.

Table 7: Results comparison between this simulation, IECM, and data from Callide oxyfuel project.

Parameter	This work	IECM	Callide [51]
Gross power (MW)	509	517	500
Net power (MW)	373	396	345
η_{gross}^{LHV} (%)	47	46	46
η_{net}^{LHV} (%)	34	35	32
O_2 demand (kg/MWh)	605	653	632
Fuel burned (kg/s)	40	46	54

The parasitic energy demand incurred by the ASU, GPU, and power plant are presented in Table 8 showing a good agreement with the values reported by Tranier *et al.* [26]

Table 8: Parasitic energy losses from ASU, GPU, and power plant from this simulation and from Tranier *et al.*

	This work	Tranier, J. P. [26]
ASU	46.2%	43.5%
GPU	33.6%	35.8%
Power plant	20.1%	20.7%

3.2. Thermodynamic analysis

The minimum thermodynamic separation work (W_{min}) associated with the ASU and GPU was calculated using Equations 6 and 7 as 5.8 kJ/mol$_{O_2}$ (49.9 kWh/t$_{O_2}$) and 0.8 kJ/mol$_{CO_2}$ (5.4 kWh/t$_{CO_2}$), respectively. The real separation work (W_{real}) required for O_2 and CO_2 was obtained from the simulation in Aspen as 24 kJ/mol$_{O_2}$ (208 kWh/t$_{O_2}$) and 15.5 kJ/mol$_{CO_2}$ (98 kWh/t$_{CO_2}$), respectively. The second law efficiency, calculated via Equation 8 allows the evaluation of the relative merit of improving the efficiency of each sub-system. On this basis, the ASU and GPU were determined to be operating with a thermodynamic efficiency of 24% and 5%, respectively.

Assuming an increase in thermodynamic efficiency of the ASU, GPU, and boiler it is possible to observe from Figure 5 that the parasitic power losses from these systems tend to decrease. A 5% increase in efficiency of the ASU results in a 17% decrease of power consumption while for the GPU results in a 46% reduction. This shows a higher increase in process efficiency with an initial improvement of the GPU, however it will be preferential to start improving the ASU once the GPU achieves a separation efficiency of 22%.
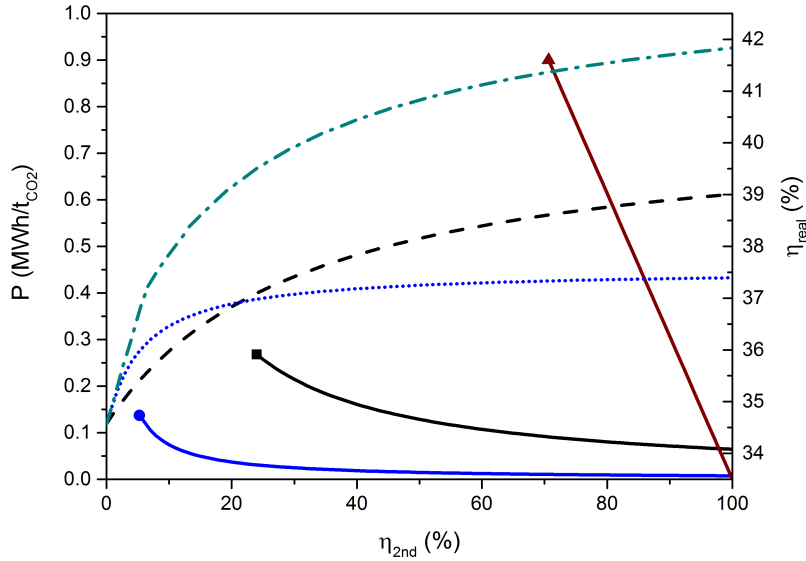
Figure 5: Effect of thermodynamic efficiency (η_{therm}) on power needed for the ASU (black line) and GPU (blue line) and for the power lost by the boiler(red line). The starting points for the ASU, GPU, and Boiler were obtained through this simulation and are represented as ■, ●, and ▲ respectively. The dashed lines represent the effect on the real efficiency of the oxy-combustion by increasing the thermodynamic efficiency of the ASU (black dashed line), the GPU (dotted blue line), and both (dash-dot cyan line). From this analysis, it can be observed that improving the GPU will lead to the greatest improvement in the overall process.

3.3. Process improvement and heat integration

The net efficiency of the simulated power plant was 34.6%. Then, assuming ideal separation of O_2 from air and CO_2 from the flue gas, the net efficiency improves to 43.1%. Tranier *et al.* [26] stated that Air Liquide can improve separation efficiency of the ASU by 10%. However, an improvement of up to 21% relative to the base simulation could be achieved by increasing the operating conditions of the boiler. The maximum thermodynamic efficiency of the power plant was 67% with a theoretical power output of 720 MW, and the minimum thermodynamic separation work for O_2 and CO_2 was 24 and 16

kJ/mol, respectively. This results in a maximum theoretical efficiency of 63% for oxy-combustion, showing that the simulated process is 55% thermodynamically efficient, represented in Figure 6.
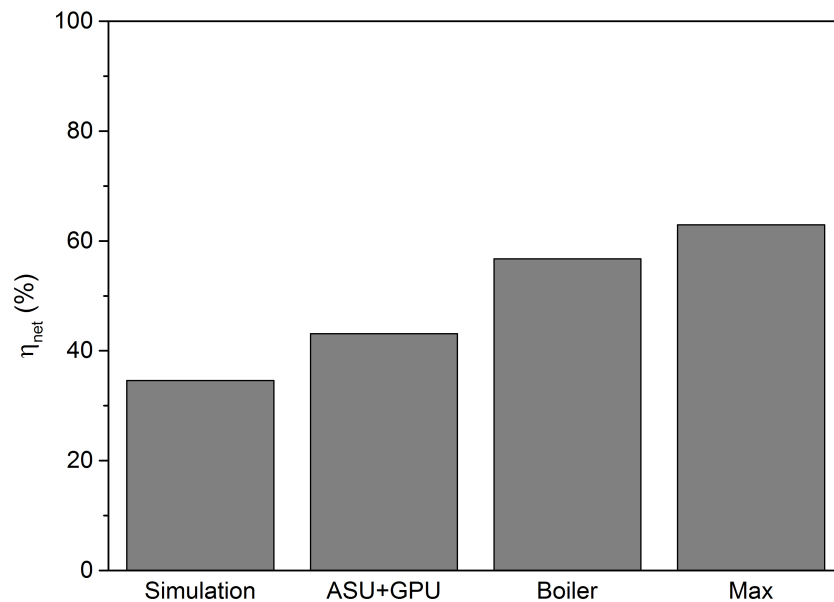

Figure 6: Comparison of the simulated oxy-combustion efficiency with the process if the ASU and GPU were operating with the minimum thermodynamic separation work (ASU+GPU), if the boiler could achieve the maximum Rankine efficiency (Boiler), and the maximum thermodynamic efficiency of the oxy-combustion process (Max). This shows the possibility for improving the process are by increasing the efficiency of the boiler, ASU, or GPU.

Advanced ultra-supercritical technology with steam parameters operating up to 700 °C and 350 bar are currently being developed [70, 71]. Such technology is able to achieve net efficiencies up to 52% on a LHV basis however, operating under such conditions is limited to current material selection [70, 71].

The exergy destruction analysis identified the boiler as the largest source of inefficiency. Due to material limitations, there are limited opportunities to improve this process element, however the feedwater heating train shows po-

tential for reducing the inefficiencies of the plant. Here, the low temperature feedwater heaters 1 to 4 were identified as an important source of inefficiency. Therefore, this is an excellent point to reuse low grade waste heat of compression from both ASU and GPU to increase the temperature of condensed feedwater. After using this low grade heat, it was found that the feedwater temperature increased sufficiently to completely bypass feedwater heaters 1 to 4, allowing for their removal as illustrated by the heat integration path in Figure 3.

The exergy destruction associated with the feedwater heating train has been significantly reduced by 53% as shown in Figure 7 due to the removal of the low pressure heaters, FWH1 to 4. This reduces the heat requirement from coal, reducing its consumption to 0.36 kg_{coal}/kWh, and increasing gross and net efficiencies to 49 and 38%, respectively.
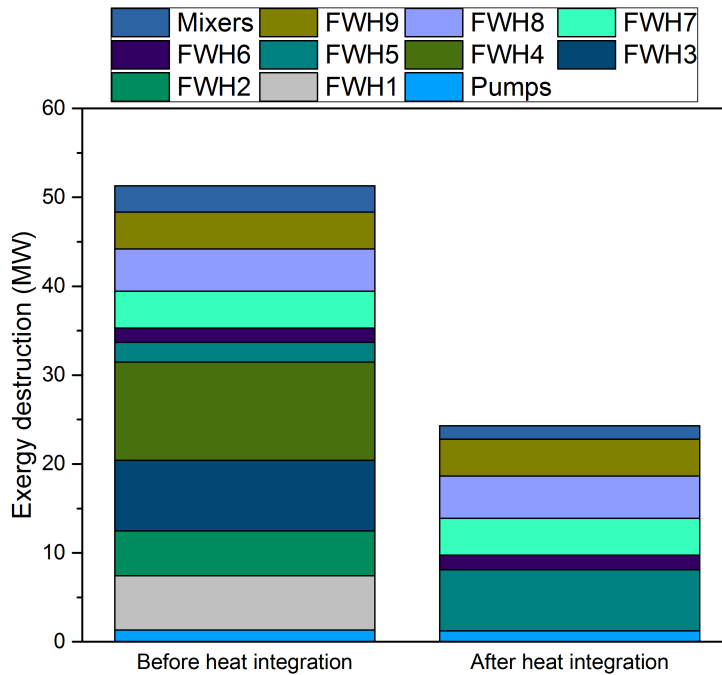
Figure 7: Exergy destruction of feedwater heating train in oxy-combustion process before and after heat integration. The reduction of exergy destruction after heat integration is because feedwater heaters FWH1 to FWH4 are removed.

The main exergy losses of the ASU were determined to be in the MHX, also identified by Taniguchi *et al.* as responsible for more than half of the exergy destroyed in the ASU [72]. Although possessing small losses (4% of total losses), the MAC was identified as a good target for heat integration as compressed air is discharged at high temperatures. An alternative is to use adiabatic compressors with one inter- and one after-cooler instead of isothermal compressors. Feedwater can be used to cool this air stream showing potential to reduce capital costs and cooling water [43].

Most exergy is destroyed in the MHX due to the high heat duty. The difference in pressure of air, at 4.2 bar, compared with the pressure of products, which are at 1.2 bar, also contribute to the exergy destruction of this unit. Decreasing

the temperature at which the air feed enters the exchanger reduced the exergy destruction of the ASU as shown in Figure 8, however that also reduces the O_2 temperature leaving the heat exchanger. Although this can negatively affect combustion efficiency, this is not a concern for oxy-combustion, and adopting this strategy will increase operational safety [14, 43].

Changing the MAC from an isothermal compressor to a two-staged adiabatic compressor has led to an increase in both exergy destruction and power consumption. This change allows to use the low grade heat of compression to pre-heat a portion of the feedwater while cooling down the compressed air stream. By using this strategy it is possible to reduce the number of feedwater heaters, as previously described.

The power consumption of both the ASU and GPU is primarily associated with the compression work. As the compressors are operating at 90% adiabatic efficiency, it will not be likely that significant increase in thermodynamic efficiency will come from improving them. One possible way of reducing the power consumption from the ASU is sending a greater amount of compressed air to the expansion turbine. Applying this strategy, the second stage of the booster was removed because the required compression could be provided using the amount of work obtained in the expander. The number of stages from the HP column was reduced to 10, and the LP column was reduced to 23 stages in order to lower the oxygen purity to 97 wt%. This strategy reduces the power consumption of the unit to 197 kWh/t_{O_2}, similar to previous work [26, 43–45, 73].
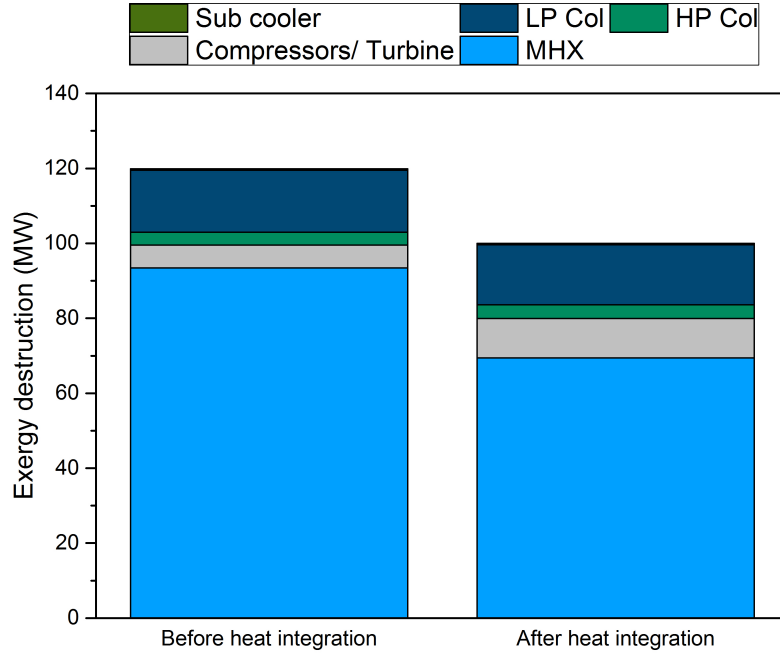
Figure 8: Exergy destruction of ASU in oxy-combustion process before and after heat integration. An increase of exergy destruction on compressors can be seen because of changing from isothermal to adiabatic compressors. On the other hand, reducing the inlet temperature of air to the main heat exchanger reduces the exergy destroyed in this unit. Overall it is observed a reduction of exergy destruction of the ASU.

The MHX was found to be where most exergy was destroyed on the GPU, as for the ASU. Low grade heat of compressed gases can be used to pre-heat feedwater [43–45, 50] however, Spero *et al.* [50] stated that some care has to be taken when employing this strategy. This is because the unit is only started when CO_2 concentrations on the flue gas are high enough to allow a successful separation. This operation could be put at risk if high concentration of impurities are present in the flue gas. One possible way of avoiding this issue is to use heat from the low pressure compression train and while CO_2 concentrations are not sufficiently high to run the process send this flue gas to the stack. This

approach has been shown by Skorek-Osikowska *et al.* [45] to provide a greater increase of net efficiency instead of using all heat of compression available in the GPU.

Changing the first compressor from a one-stage to a two-staged compressor with inter-cooling has reduced the exergy destruction of the unit. This strategy also reduces the power required by the compressor and avoids increasing the gas temperature to levels that could reduce the equipment lifetime. Low grade heat of compression is used to pre-heat another portion of the feedwater and cool down the compressed flue gas. The second compressor uses the rest of the feedwater to cool down the compressed flue gas, while using its heat to increase the feedwater temperature. This allowed for a 6.4% decrease of exergy destruction in the GPU obtaining a final CO_2 stream with 99 wt% purity at a specific power consumption of 137 kWh/t$_{CO_2}$, considering the final CO_2 compression to pipeline pressure.

In summary, a 4% decrease of exergy destruction is observed after process optimisation and heat integration between the power plant and both ASU and GPU.

3.4. Techno-economic analysis

The results from the thermodynamic and exergetic analysis show that the changes proposed to the process have improved the efficiency of the plant. To analyse if these changes would be economically appealing, the efficiency was plotted against CAPEX as represented in Figure 9. This enables a comparison with the baselines, chosen to be the unabated power plant CAPEX and the maximum thermodynamic efficiency determined earlier. The ideal path for technological innovation is represented by the arrow in Figure 9 going from the oxy-combustion before improvement towards where the baselines cross. A reduction of CAPEX from £436M to £369M and an increase of net efficiency from 34% to 37% is observed, resulting in a decrease of 13% in £/MWh.
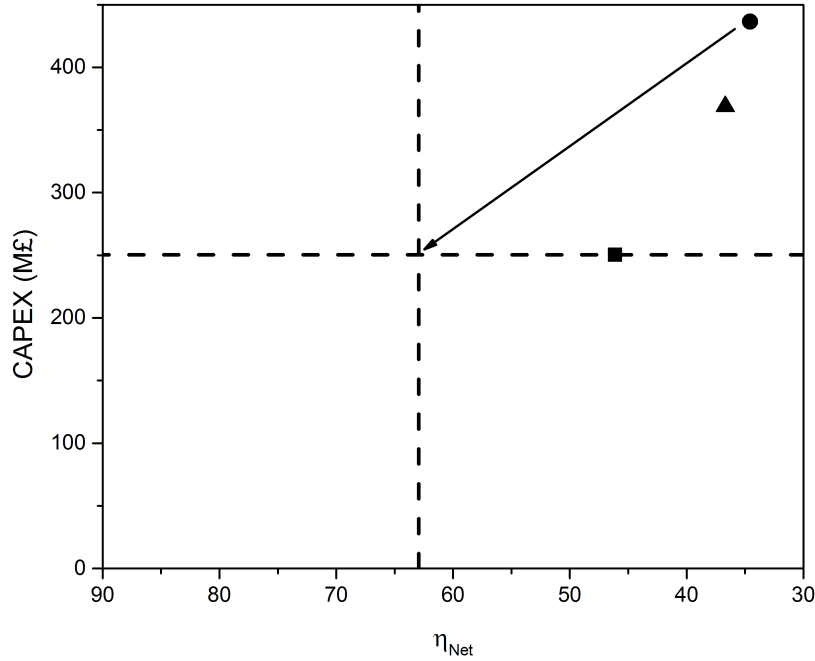
28

Figure 9: Plant efficiency plotted against CAPEX, ■ represents the unabated power plant, ●
the oxy-combustion before process improvement and ▲ after process improvement. The horizontal dashed line represents the CAPEX of the unabated power plant, and the vertical dashed
line the maximum thermodynamic efficiency. The desired direction of process improvement is
represented by the arrow, showing both an increase of efficiency and a reduction of CAPEX.
The process improvement using this analysis reduced CAPEX and increased efficiency, but
showed a sharper reduction of CAPEX than increase in efficiency.

4. Conclusions

The methodology proposed in this study is illustrated in Figure 10 and was
successful in identifying opportunities for the concurrent improvement in process
efficiency and reduction in capital cost of an oxy-combustion power plant.
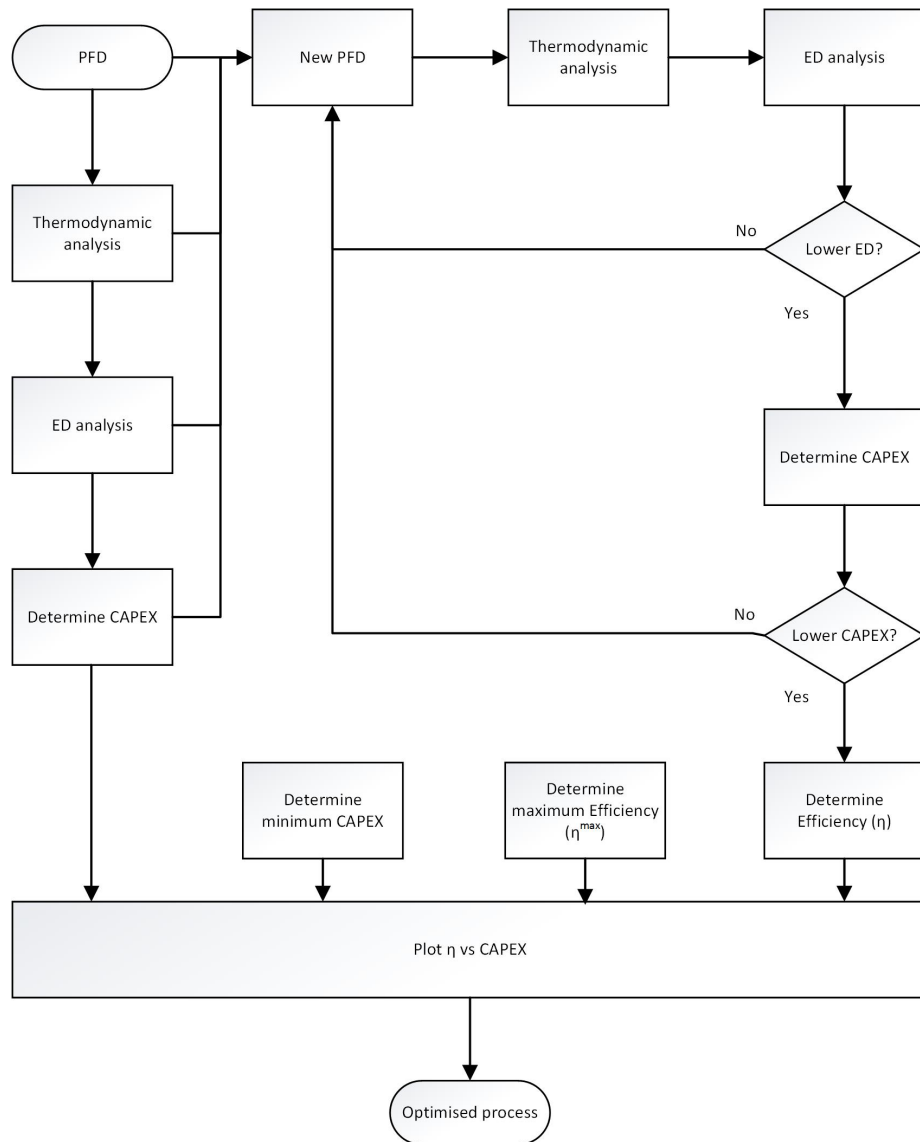
29

Figure 10: Methodology proposed for process improvement using first and second laws of thermodynamics, followed by an exergy destruction (ED) and CAPEX analysis.

In this study, heat integration between the feedwater heating train and the compressors in the ASU and GPU allowed the removal of the low pressure feed-

water heaters, reducing the amount of steam bleed from the LP steam turbine, thus increasing the amount of electricity generated. This has the dual benefits of reduced capital cost and improved power generation efficiency. Moreover, this heat integration strategy would reduce the water intensity of the CCS plant, resulting in a smaller cooling tower, land use, and capital cost.

The minimum thermodynamic separation work for the ASU to obtain the desired oxygen purity of 97 wt% was found to be 49.9 kWh/t_{O_2} and for the GPU to obtain a CO_2 purity of 99.9 wt% was 5.4 kWh/t_{CO_2}. After heat integration the power consumption of the ASU was reduced by 3.4% to 197 kWh/t_{O_2} and the GPU by 2.1% to 137 kWh/t_{CO_2}, representing a second law efficiency of 24% and 5%, respectively.

On the basis of this analysis, the maximum Rankine efficiency of the boiler simulated in this study was 66.8% and the maximum theoretical efficiency of the oxy-combustion process was 62.3% LHV. Owing to the low efficiency of the GPU relative to the ASU, focusing on improving the Second Law efficiency was observed to be a promising option for improving the efficiency of the oxy-combustion process.

Finally, using this approach, the net efficiency of the oxy-combustion was increased by 3% to 37% LHV, with a CAPEX reduction of 15%, and reduced the £/MWh by 13%.

This work is therefore of general use to anyone proposing a new power generation or storage technology and provides a rational basis for its evaluation and comparison with incumbent options.

Nomenclature

ASU	Air Separation Unit
CAPEX	Capital Expenditure
CCS	Carbon Capture and Storage
DCC	Direct Contact Cooler
ED	Exergy Destruction

F_{80}	Mean particle size of coal feed to grinder
FWH	Feedwater Heater
G	Coal grindability
GPU	Gas Processing Unit
h	Specific enthalpy
HP	High Pressure
HX	Heat Exchanger
IP	Intermediate Pressure
LHV	Lower Heating Value
LP	Low Pressure
MAC	Main Air Compressor
MHX	Multiple-stream heat exchanger
n	Molar flow
NGCC	Natural gas combined cycle
P_1	Target particle size of grinding process
P_{80}	Mean particle size at grinder outlet
PFD	Process Flow Diagram
Q	Heat flow
RFG	Recycled flue gas
SD	Spray Dryer
R	Perfect Gas Constant
RS	Radiant Superheater
RH	Reheater
RHX	Regenerative heat exchanger
s	Specific enthropy
SH	Superheater
T	Temperature
T_{ad}	Adiabatic flame temperature
W	Work
W_i	Bond Work Index

W_{min}	Minimum separation work
y	molar fraction
η_{gross}	Gross efficiency of the plant
η_{net}	Net efficiency of the plant

References

[1] C. L. Quéré, R. Moriarty, R. M. Andrew, J. G. Canadell, S. Sitch, J. I. Korsbakken, P. Friedlingstein, G. P. Peters, R. J. Andres, T. A. Boden, R. A. Houghton, J. I. House, R. F. Keeling, P. Tans, A. Arneth, D. C. E. Bakker, L. Barbero, L. Bopp, J. Chang, F. Chevallier, L. P. Chini, P. Ciais, M. Fader, R. A. Feely, T. Gkritzalis, I. Harris, J. Hauck, T. Ilyina, A. K. Jain, E. Kato, V. Kitidis, K. K. Goldewijk, C. Koven, P. Landschützer, S. Lauvset, N. Lefévre, A. Lenton, I. D. Lima, N. Metzl, F. Millero, D. R. Munro, A. Murata, J. Nabel, S. Nakaoka, Y. Nojiri, K. O'Brien, A. Olsen, T. Ono, F. F. Pérez, B. Pfeil, D. Pierrot, B. Poulter, G. Rehder, C. Rödenbeck, S. Saito, U. Schuster, J. Schwinger, R. Séférian, T. Steinhoff, B. D. Stocker, A. J. Sutton, T. Takahashi, B. Tilbrook, I. T. van der Laan-Luijkx, G. R. van der Werf, S. van Heuven, D. Vandemark, N. Viovy, A. Wiltshire, S. Zaehle, N. Zeng, Global carbon budget 2015, Earth System Science Data 7 (2015) 349–396.

[2] J. G. Olivier, G. Janssens-Maenhout, M. Muntean, J. A. Peters, Trends in global CO_2 emissions, Report, The Hague: PBL Netherlands Environmental Assessment Agency, Ispra: European Commission, Joint Research Centre (2016).

[3] O. Edenhofer, R. Pichs-Madruga, Y. Sokona, S. Kadner, J. C. Minx, S. Brunner, S. Agrawala, G. Baiocchi, I. A. Bashmakov, G. Blanco, J. Broome, T. Bruckner, M. Bustamante, L. Clarke, M. C. Grand, F. Creutzig, X. C.-N. nez, S. Dhakal, N. K. Dubash, P. Eickemeier, E. Farahani, M. Fischedick, M. Fleurbaey, R. Gerlag, L. Gómez-Echeverri,

S. Gupta, J. Harnisch, K. Jiang, F. Jotzo, S. Kartha, S. Klasen, C. Kolstad, V. Krey, H. Kunreuther, O. Lucon, O. Masera, Y. Mulugetta, R. Norgaard, A. Patt, N. H. Ravindranath, K. Riahi, J. Roy, A. Sagar, R. Schaeffer, S. Schlömer, K. Seto, K. Seyboth, R. Sims, P. Smith, E. Somanathan, R. Stavins, C. von Stechow, T. Sterner, T. Sugiyama, S. Suh, K. Urama, D. Ürge Vorsatz, A. Venables, D. G. Victor, E. Weber, D. Zhou, J. Zou, T. Zwickel, Climate change 2014: Mitigation of climate change. contribution of working group III to the fifth assessment report of the intergovernmental panel on climate change, Technical summary, Cambridge University Press, Cambridge, United Kingdom and New York, NY, USA (2014).

[4] BP statistical review of world energy 2017, Report, BP p.l.c. (2017).

[5] B. Buhre, L. Elliott, C. Sheng, R. Gupta, T. Wall, Oxy-fuel combustion technology for coal-fired power generation, Progress in Energy and Combustion Science 31 (4) (2005) 283–307.

[6] N. Mac Dowell, N. Florin, A. Buchard, J. Hallett, A. Galindo, G. Jackson, C. S. Adjiman, C. K. Williams, N. Shah, P. Fennell, An overview of CO_2 capture technologies, Energy & Environmental Science 3 (11) (2010) 1645–1669.

[7] M. E. Boot-Handford, J. C. Abanades, E. J. Anthony, M. J. Blunt, S. Brandani, N. Mac Dowell, J. R. Fernández, M.-C. Ferrari, R. Gross, J. P. Hallett, R. S. Haszeldine, P. Heptonstall, A. Lyngfelt, Z. Makuch, E. Mangano, R. T. J. Porter, M. Pourkashanian, G. T. Rochelle, N. Shah, J. G. Yao, P. S. Fennell, Carbon capture and storage update, Energy & Environmental Science 7 (1) (2014) 130–189.

[8] S. M. Benson, Carbon capture and storage, in: Global Energy Assessment - Toward a Sustainable Future, Cambridge University Press, Cambridge, UK, 2012, Ch. 13, pp. 993–1068.

[9] D. J. Dillon, V. White, R. J. Allam, R. A. Wall, J. Gibbins, Oxy combustion

processes for CO_2 capture from power plant, Tech. Rep. 2005/9, Mitsui Babcock Energy Limited.

[10] Y. Le Moullec, Assessment of carbon capture thermodynamic limitation on coal-fired power plant efficiency, International Journal of Greenhouse Gas Control 7 (2012) 192–201.

[11] A. Chansomwong, K. Zanganeh, A. Shafeen, P. Douglas, E. Croiset, L. Ricardez-Sandoval, Dynamic modelling of a CO_2 capture and purification unit for an oxy-coal-fired power plant, International Journal of Greenhouse Gas Control 22 (2014) 111 – 122.

[12] C. Yin, J. Yan, Oxy-fuel combustion of pulverized fuels: Combustion fundamentals and modeling, Applied Energy 162 (2016) 742 – 762.

[13] Oxyfuel combustion of pulverised coals, Tech. Rep. 2010/07, IEA GHG.

[14] C. E. Baukal Jr., Oxygen-Enhanced Combustion, 2nd Edition, CRC Press.

[15] C. Fu, R. Anantharaman, K. Jordal, T. Gundersen, Thermal efficiency of coal-fired power plants: From theoretical to practical assessments, Energy Conversion and Management 105 (2015) 530–544.

[16] C. Kolster, E. Mechleri, S. Krevor, N. Mac Dowell, The role of CO_2 purification and transport networks in carbon capture and storage cost reduction, International Journal on Greenhouse Gas Control 58 (2017) 127 – 141.

[17] A. Smith, J. Klosek, A review of air separation technologies and their integration with energy conversion processes, Fuel Processing Technology 70 (2) (2001) 115–134.

[18] A. Darde, R. Prabhakar, J.-P. Tranier, N. Perrin, Air separation and flue gas compression and purification units for oxy-coal combustion systems, Energy Procedia 1 (1) (2009) 527 – 534.

[19] C. Linde, Process of producing low temperatures, the liquefaction of gases, and the separation of the constituents of gaseous mixtures. US Patent 727,650 (May 12 1903).

[20] R. F. Barron, Cryogenic systems, 2nd Edition, Oxford University Press, 1985.

[21] N. A. Downie, Industrial gases, London: Blackie Academic & Professional, 1996.

[22] M. J. Kirschner, Oxygen, in: Ullmann's Encyclopedia of Industrial Chemistry, John Wiley and Sons, Inc., 2000.

[23] D. W. Green, R. H. Perry, Cryogenic processes, in: Perry's Chemical Engineers' Handbook, eighth Edition, John Wiley and Sons, Inc., 2008, Ch. 11: Heat transfer Equipment.

[24] V. N. Raibhole, S. N. Sapali, Simulation and parametric analysis of cryogenic oxygen plant for biomass gasification, Mechanical Engineering Research 2 (2) (2012) 97–107.

[25] S. N. Sapali, V. N. Raibhole, Exergy analysis of cryogenic air separation unit integrated with biomass gasifier, in: Proceedings of the World Congress on Engineering and Computer Science, Vol. II, 2013.

[26] J. P. Tranier, R. Dubettier, A. Darde, N. Perrin, Air separation, flue gas compression and purification units for oxy-coal combustion systems, Energy Procedia 4 (4) (2011) 966–971.

[27] Q. Fu, Y. Kansha, C. Song, Y. Liu, M. Ishizuka, A. Tsutsumi, A cryogenic air separation process based on self-heat recuperation for oxy-combustion plants, Applied Energy 162 (2016) 1114 – 1121.

[28] M. W. Ackley, S. U. Rege, H. Saxena, Application of natural zeolites in the purification and separation of gases, Microporous and Mesoporous Materials 61 (1–3) (2003) 25 – 42.

[29] P. Li, F. H. Tezel, Adsorption separation of N_2, O_2, CO_2 and CH_4 gases by β-zeolite, Microporous and Mesoporous Materials 98 (1–3) (2007) 94 – 101.

[30] J. T. Chen, C. C. Shih, Y. J. Fu, S. H. Huang, C. C. Hu, K. R. Lee, J. Y. Lai, Zeolite-filled porous mixed matrix membranes for air separation, Industrial & Engineering Chemistry Research 53 (7) (2014) 2781–2789.

[31] J. F. Vente, W. G. Haije, R. IJpelaan, F. T. Rusting, On the full-scale module design of an air separation unit using mixed ionic electronic conducting membranes, Journal of Membrane Science 278 (1–2) (2006) 66 – 71.

[32] R. Castillo, Thermodynamic analysis of a hard coal oxyfuel power plant with high temperature three-end membrane for air separation, Applied Energy 88 (5) (2011) 1480 – 1493.

[33] S. Hashim, A. Mohamed, S. Bhatia, Oxygen separation from air using ceramic-based membrane technology for sustainable fuel production and power generation, Renewable and Sustainable Energy Reviews 15 (2) (2011) 1284 – 1293.

[34] R. Wang, B. Meng, X. Meng, X. Tan, J. Sunarso, L. Liu, S. Liu, Highly stable $La_{0.6}Sr_{0.4}Co_{0.2}Fe_{0.8}O_{3-\delta}$ hollow fibre membrane for air separation swept by steam or steam mixture, Journal of Membrane Science 479 (2015) 232 – 239.

[35] K. Mezghani, A. Hamza, Application of $Ba_{0.5}Sr_{0.5}Co_{0.8}Fe_{0.2}O_{3-\delta}$ membranes in an oxy-fuel combustion reactor, Journal of Membrane Science 518 (2016) 254 – 262.

[36] K. Shah, B. Moghtaderi, T. Wall, Effect of flue gas impurities on the performance of a chemical looping based air separation process for oxy-fuel combustion, Fuel 103 (2013) 932 – 942.

[37] K. Wang, Q. Yu, Q. Qin, Reduction kinetics of Cu-based oxygen carriers for chemical looping air separation, Energy & Fuels 27 (9) (2013) 5466–5474.

[38] C. Zhou, K. Shah, B. Moghtaderi, Techno-economic assessment of integrated chemical looping air separation for oxy-fuel combustion: An australian case study, Energy & Fuels 29 (4) (2015) 2074–2088.

[39] D. R. Vinson, Air separation control technology, Computers & Chemical Engineering 30 (10–12) (2006) 1436 – 1446, papers form Chemical Process Control VIICPC VII international conference in the Series.

[40] A. Skorek-Osikowska, Łukasz Bartela, J. Kotowicz, Thermodynamic and ecological assessment of selected coal-fired power plants integrated with carbon dioxide capture, Applied Energy 200 (2017) 73 – 88.

[41] F. Abdollahi-Demneh, M. A. Moosavian, M. R. Omidkhah, H. Bahmanyar, Calculating exergy in flowsheeting simulators: A HYSYS implementation, Energy 36 (8) (2011) 5320 – 5327, PRES 2010.

[42] T. Kotas, Exergy concepts for thermal plant, International Journal of Heat and Fluid Flow 2 (3) (1980) 105 – 114.

[43] Improved oxygen production technologies, Tech. Rep. 2007/14, IEA Greenhouse Gas R&D Programme (IEA GHG).

[44] H. Hagi, Y. L. Moullec, M. Nemer, C. Bouallou, Performance assessment of first generation oxy-coal power plants through an exergy-based process integration methodology, Energy 69 (2014) 272 – 284.

[45] A. Skorek-Osikowska, L. Bartela, J. Kotowicz, M. Job, Thermodynamic and economic analysis of the different variants of a coal-fired, 460 MW power plant using oxy-combustion technology, Energy Conversion and Management 76 (2013) 109 – 120.

[46] M. Aneke, M. Wang, Process analysis of pressurized oxy-coal power cycle for carbon capture application integrated with liquid air power generation and binary cycle engines, Applied Energy 154 (2015) 556 – 566.

[47] R. Stanger, L. Belo, T. Ting, C. Spero, T. Wall, Mercury and SO_3 measurements on the fabric filter at the callide oxy-fuel project during air and oxy-fuel firing transitions, International Journal of Greenhouse Gas Control 47 (2016) 221 – 232.

[48] S. Li, H. Li, W. Li, M. Xu, E. G. Eddings, Q. Ren, Q. Lu, Coal combustion emission and ash formation characteristics at high oxygen concentration in a 1mwth pilot-scale oxy-fuel circulating fluidized bed, Applied Energy 197 (2017) 203 – 211.

[49] B. Oboirien, V. Thulari, B. North, Enrichment of trace elements in bottom ash from coal oxy-combustion: Effect of coal types, Applied Energy 177 (2016) 81 – 86.

[50] C. Spero, F. Montagner, L. Chapman, D. Ranie, T. Yamada, Callide oxy-fuel project – lessons learned, Tech. Rep. 2014, Global CCS Institute.

[51] A. Komaki, T. Gotou, T. Uchida, T. Yamada, T. Kiga, C. Spero, Operation experiences of oxyfuel power plant in Callide oxyfuel project, Energy Procedia 63 (2014) 490–496.

[52] D. Liu, T. Wall, R. Stanger, CO_2 quality control in oxy-fuel technology for CCS: SO_2 removal by the caustic scrubber in Callide oxy-fuel project, International Journal of Greenhouse Gas Control 51 (2016) 207 – 217.

[53] J. Monne, L. Jammes, E. Gaucher, N. Labat, C. Urbancyk, S. Thibeau, C. Prinet, X. Payre, T. Schuhler, D. Pourtoy, D. Copin, Carbon capture and storage: the Lacq pilot, Tech. Rep. 2015, Total S. S.

[54] Endesa, Ciuden, Foster Wheeler, Briscnet Ibérica, P. G. Cerezales, M. A. Fernández, OXYCFB300 Compostilla, carbon capture and storage demonstration project, knowledge sharing FEED report, Tech. Rep. 2013, Endesa, Madrid.

[55] L. Strömberg, G. Lindgren, J. Jacoby, R. Giering, M. Anheden, U. Burchhardt, H. Altmann, F. Kluger, G.-N. Stamatelopoulos, Update on Vatten-

fall's 30 MWth oxyfuel pilot plant in Schwarze Pumpe, Energy Procedia 1 (1) (2009) 581–589.

[56] M. Anheden, U. Burchhardt, H. Ecke, R. Faber, O. Jidinger, R. Giering, H. Kass, S. Lysk, E. Ramström, J. Yan, Overview of operational experience and results from test activities in Vattenfall's 30 MWth oxyfuel pilot plant in Schwarze Pumpe, Energy Procedia 4 (2011) 941–950.

[57] O. Williams, C. Eastwick, S. Kingman, D. Giddings, S. Lormor, E. Lester, Investigation into the applicability of bond work index (BWI) and hardgrove grindability index (HGI) tests for several biomasses compared to colombian La Loma coal, Fuel 158 (2015) 379 – 387.

[58] E. S. Rubin, H. Zhai, K. Kietzke, H. Mantripragada, Integrated Environmental Control Model, version 9.2.1, Public release; Carnegie Mellon University: Pittsburgh, PA, 2016, `http://www.cmu.edu/epp/iecm/` (2016).

[59] W. Castle, Air separation and liquefaction: recent developments and prospects for the beginning of the new millennium, International Journal of Refrigeration 25 (1) (2002) 158–172.

[60] H. Spliethoff, Power generation from solid fuels, Springer-Verlag Berlin Heidelberg, 2010.

[61] J. Ciferno, Pulverized coal oxycombustion power plants, Tech. Rep. DOE/NETL-2007/1291, National Energy Technology Laboratory.

[62] S. Posch, M. Haider, Optimization of CO_2 compression and purification units (CO_2CPU) for CCS power plants, Fuel 101 (2012) 254 – 263.

[63] V. White, L. Torrente-Murciano, D. Sturgeon, D. Chadwick, Purification of oxyfuel-derived CO_2, International Journal of Greenhouse Gas Control 4 (2) (2010) 137 – 142, the Ninth International Conference on Greenhouse Gas Control Technologies.

[64] F. Carrasco-Maldonado, R. Spörl, K. Fleiger, V. Hoenig, J. Maier, G. Scheffknecht, Oxy-fuel combustion technology for cement production – State of the art research and technology development, International Journal of Greenhouse Gas Control 45 (2016) 189 – 199.

[65] T. Wall, R. Stanger, S. Santos, Demonstrations of coal-fired oxy-fuel technology for carbon capture and storage and issues with commercial deployment, International Journal of Greenhouse Gas Control 5, Supplement 1 (2011) S5 – S15, Oxyfuel Combustion Technology - Working Toward Demonstration and Commercialisation.

[66] R. Stanger, T. Wall, R. Spörl, M. Paneru, S. Grathwohl, M. Weidmann, G. Scheffknecht, D. McDonald, K. Myöhänen, J. Ritvanen, S. Rahiala, T. Hyppänen, J. Mletzko, A. Kather, S. Santos, Oxyfuel combustion for CO_2 capture in power plants, International Journal of Greenhouse Gas Control 40 (2015) 55–125.

[67] J. Wilcox, Carbon Capture, Springer Science+Business Media, LL.C, 2012.

[68] R. T. Porter, M. Fairweather, C. Kolster, N. Mac Dowell, N. Shah, R. M. Woolley, Cost and performance of some carbon capture technology options for producing different quality CO_2 product streams, International Journal of Greenhouse Gas Control 57 (2017) 185 – 195.

[69] M. Lackner, Combustion science and technology, in: Kirk-Othmer Encyclopedia of Chemical Technology, John Wiley & Sons, Inc., 2000.

[70] P. S. Weitzel, J. M. Tanzosh, B. Boring, N. Okita, N. Takahashi, T. Ishikawa, Advanced ultra-supercritical power plant (700 to 760C) design for indian coal, Tech. Rep. BR-1884.

[71] K. Nicol, Status of advanced ultra-supercritical pulverised coal technology, Tech. Rep. CCC/229, IEA Clean Coal Centre (2013).

[72] M. Taniguchi, H. Asaoka, T. Ayuhara, Energy saving air-separation plant based on exergy analysis, Kobelco Technology Review No.33.

[73] P. Higginbotham, V. White, K. Fogash, G. Guvelioglu, Oxygen supply for oxyfuel CO_2 capture, International Journal of Greenhouse Gas Control 5, Supplement 1 (2011) S194 – S203, Oxyfuel Combustion Technology - Working Toward Demonstration and Commercialisation.